Princeton Plasma Physics Laboratory

PPPL-4089

PPPL-4089

Observation of Abrupt- and Fast-rising SOL Current during Trigger Phase of ELMs in DIII-D Tokamak

H. Takahashi, E. Fredrickson, M. Schaffer, M. Austin, N. Brooks,
T. Evans, G. Jackson, L. Lao, and J. Watkins

June 2005

Prepared for the U.S. Department of Energy under Contract DE-AC02-76CH03073.

PPPL Report Disclaimers

Full Legal Disclaimer

Trademark Disclaimer

PPPL Report Availability

This report is posted on the U.S. Department of Energy's Princeton Plasma Physics Laboratory Publications and Reports web site in Fiscal Year 2005. The home page for PPPL Reports and Publications is: http://www.pppl.gov/pub_report/

Office of Scientific and Technical Information (OSTI):

Available electronically at: http://www.osti.gov/bridge.

Available for a processing fee to U.S. Department of Energy and its contractors, in paper from:

U.S. Department of Energy
Office of Scientific and Technical Information
P.O. Box 62
Oak Ridge, TN 37831-0062

Telephone: (865) 576-8401

Fax: (865) 576-5728

E-mail: reports@adonis.osti.gov

National Technical Information Service (NTIS):

This report is available for sale to the general public from:

U.S. Department of Commerce
National Technical Information Service
5285 Port Royal Road
Springfield, VA 22161

Telephone: (800) 553-6847

Fax: (703) 605-6900

Email: orders@ntis.fedworld.gov

Online ordering: http://www.ntis.gov/ordering.htm

Observation of Abrupt- and Fast-rising SOL Current during Trigger Phase of ELMs in DIII-D Tokamak

H. Takahashi[1], E.D. Fredrickson[1], M.J. Schaffer[2], M.E. Austin[3], N.H. Brooks[2], T.E. Evans[2], G.L. Jackson[2], L.L. Lao[2], and J.G. Watkins[4]

[1]*Princeton University, Princeton, New Jersey USA*
[2]*General Atomics, San Diego, California USA*
[3]*University of Texas, Austin, Texas USA*
[4]*Sandia National Laboratory, Albuquerque, New Mexico USA*

Extensive studies (see, e.g., ref. [1]) to date of edge localized modes (ELMs) have sought their *origin* inside the separatrix, i.e., MHD instability from steep gradients in the plasma edge, and examined their *consequences* outside the separatrix, i.e., transport of heat and particles in the scrape-off-layer (SOL) and divertors. Recent measurement by a high-speed scrape-off-layer current (SOLC) diagnostic may indicate that the ELM trigger process lies, in part, in the SOL. Thermoelectrically driven SOLC precedes, or co-evolves with, other parameters of the ELM process, and thus can potentially play a causal role: error field generated by non-axisymmetric SOLC, flowing in the immediate vicinity (~1 cm) of the plasma edge, may contribute toward destabilizing MHD modes. The SOLC, observed concurrently with MHD activity, including ELMs, has been reported elsewhere [2].

I. SOLC as ELM Precursor

Figure 1 compares onset times of an ELM in a lower single null (LSN) discharge in DIII-D as observed in signals from five diagnostics commonly used to identify ELMs. (Diagnostics used in this experiment are described and referenced in [2].) The ELM onset time for each signal is shown by a gray band in Fig. 1, as noise in the signal makes a precise determination difficult. The period before the ELM shows the noise level in the absence of an ELM. The SOLC onset is among the earliest of the common ELM signatures shown in Fig. 1, and in the precursor phase of the ELM process. This observation is contrary to the usual notion that the SOLC increases as a *consequence* of an ELM when an MHD instability ejects heat and particles into the SOL from the main plasma. In particular, a thermal collapse, as evidenced by a sudden drop in electron temperature (T_e) near the pedestal top, occurs later than the SOLC onset by ~90 μs in this ELM. At other toroidal locations the SOLC evolves differently, transforming an approximately uniform toroidal distribution before the onset into a non-axisymmetric one [3]. Magnetic field perturbations ($\dot{B}$) begin approximately coincident with the SOLC change. Onset in the D_α light is later than the thermal collapse in this ELM. D_α light from 14 locations in the top and bottom divertors has also been examined (not shown). In all cases the onset is delayed from the SOLC by 50-100 μs. Onset in SXR is approximately coincident with the thermal collapse. These general characteristics of the timing of SOLC onset with respect to the other commonly observed signatures of the ELM are also born out in examinations of other ELMs in DIII-D. The SOLC onset typically leads thermal collapse by 60-200 μs. The ELM cycle is a repetitive chain of causal events, each link in the chain causing the next one to occur. The SOLC precursor is but one of the many links. As γ rises for a given value of Θ, an increasingly larger fraction of thermoelectric potential appears across the ion sheath, as demonstrated below.

II. Ion Saturation Current Density Limitation

The observations above demonstrate that the initial abrupt and rapid increase in the SOLC is in the precursor phase of the ELM process; however, after a thermal collapse, SOLC evolution may be closely tied with that of heat and particles in the SOL and divertors. But they also raise the question of how the SOLC can rise in the face of constraints imposed on its magnitude by the ion saturation current limit at the sheath – a question that would not have arisen, had the observed SOLC increase occurred only *after* the thermal collapse.

Figure 2 shows evolution of the ion saturation current density ($j_{sat} \propto n_i \sqrt{T_e}$ where n_i and T_e are the ion density and electron temperature at the sheath) over a period including three ELMs. j_{sat} increased (in a negative domain) in a spiky manner at each ELM, and then plummeted to what appears to be a limiting value at which point the next ELM occurred. This robust cyclical process represents mainly a sharp increase in ion density at divertor plates after a thermal collapse, followed by pump-out. The limiting current, just before each of the three ELMs shown in the figure, was $j_{sat} \sim 3.5$ A/cm^2. This value is comparable to the current density during the quiescent period before an ELM, estimated from the total current flowing through an unbiased tile current sensor [2] together with a separately determined SOLC radial profile. For an abrupt and substantial increase in the SOLC to occur just before the ELM thermal collapse, the ion saturation current limitation must be lifted. Breakdown of the sheath, caused by excessive voltage imposed across it, is a candidate mechanism for momentary lifting of the limitation. By searching for experimental evidence for sheath breakdown the hypothesis may be tested that SOLC may play a role in ELM onset.

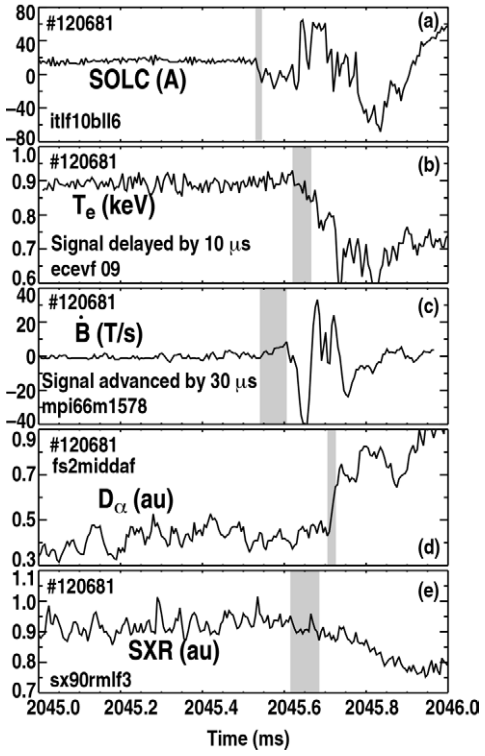

Fig. 1. ELM onset timing determined by various diagnostics: (a) SOLC signal from a sensor, measuring current through a single tile (out of 48 in toroidal array), that shows the earliest onset in a 7-sensor toroidal array, (b) T_e measured by the electron cyclotron emission (ECE) diagnostic near the top of the T_e pedestal, ~3 cm inside the separatrix in the outboard midplane, (c) magnetic field signal ($\dot{B}$) from one of several Mirnov coils that show the earliest onset among 35 coils distributed in a toroidal and poloidal array, (d) chord-integrated D_α light signal from a tangential sight line (toroidal) passing through a point ~1 cm outside the separatrix just below the outboard midplane, (e) chord-integrated soft x-ray (SXR) signal from a sight line (poloidal) through the "shoulder" region, ~3 cm inside the separatrix above the outboard midplane. The relative timing of the signals was adjusted by recording a common reference signal in their digitizers

III. Thermoelectrically Driven SOLC

Harbour [4] observed current flowing from a target plate in a higher-T_e divertor ("hot sheath") to a plate in a lower-T_e divertor ("cold sheath") in JET, and provided a theoretical interpretation for the current based on the thermoelectric potential arising from the difference in temperature at the two sheaths. Staebler and Hinton [5] extended his analysis to include finite resistance of the SOL region connecting the two sheaths. The present article adopts the latter formulation to build a thermoelectric circuit model depicted in Fig. 3. The SOLC flows

along open field lines in the SOL, enters a structural component, e.g., divertor plate, through a sheath formed at the plasma-structure interface, and may complete its circuit through vacuum vessel walls, or re-emerge onto another set of open field lines. SOLC circuit impedance arises mainly from resistance in the SOL plasma and at the sheaths.

The density of current (j) flowing through a flux tube from a hot sheath (electron temperature T_h) to a cold sheath (T_c), normalized by the ion saturation current density (j_{sat}) at the cold sheath, is denoted by $\hat{j}$ (with Staebler and Hinton sign conventions, $-1 < \hat{j} \le 0$), and the potentials at the hot and cold sheath edges, normalized by T_c (in units of eV), are $\hat{\phi}_h$ and $\hat{\phi}_c$, respectively. These variables are governed by a set of three equations shown in Fig. 3(c), which depends on two dimensionless system parameters: γ is the ratio of a limiting value of the resistance of a unit area of ion sheath, defined by $T_c/|j|$ as $|j| \rightarrow j_{sat}$, to the resistance of a flux tube of unit area in the SOL, and $\Theta \equiv T_h/T_c$ is the hot-to-cold-sheath T_e ratio. ϕ_0 is an externally applied potential, included for completeness but not considered in the present analysis. The equations involve two other constants: $\varsigma \equiv 0.85 - \lambda_{11}/\lambda_{12}$ (= 0.703 for D_2), where λ_{11} and λ_{12} are Spitzer-Härm coefficients, and $\kappa \equiv (1/2)\ln(2m_i/\pi m_e)$ (=3.89 for D_2), where m_i and m_e are the ion and electron mass. As γ rises for a given value of Θ, an increasingly larger fraction of thermoelectric potential appears across the ion sheath, as demonstrated below.

IV. Potential Drop Across Ion Sheath

The solution of governing equations for $\hat{\phi}_c$ as function of γ and Θ is shown as a contour plot in Fig. 4. The contour in the bottom left corner region of the plot ("flat land") is for $\hat{\phi}_c = 4$, just above the value, κ, attained in the absence of a thermoelectric effect. The top right region of the plot ("hills"), with higher sheath potential, may be expected to be more prone to sheath breakdown,

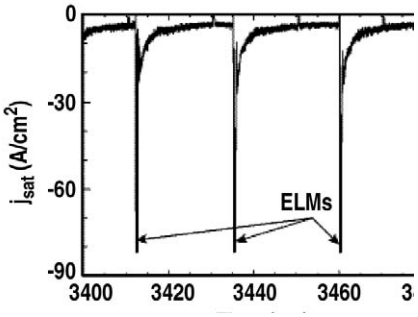

Fig. 2 j_{sat} evolution in an ELMing H-mode period measured by a strongly negatively biased Langmuir probe in the outboard bottom divertor in an LSN discharge. The probe was on a flux surface ~6.1 cm away from the strike point on the SOL side as measured along the divertor plate (~1.3 cm from the separatrix when mapped to the outboard midplane). The signal is inverted and saturated at its peaks.

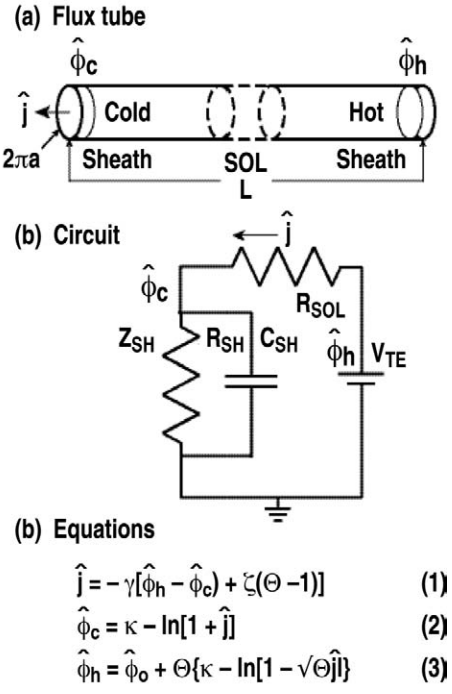

Fig. 3. Thermoelectric circuit model: (a) flux tube formed by open helical field lines in the SOL idealized as a straight circular cross-section cylinder of length "L" and radius "a," having uniform properties within. Each end of flux tube terminates at a divertor plate where a plasma sheath is formed, (b) equivalent circuit. Thermoelectric potential (V_{TE}) is shared between two resistors in series forming a voltage divider, a linear SOL resistor (R_{SOL}) and a nonlinear sheath ("ion sheath") resistor (R_{SH}) at the cold sheath, where ion current (positive charge) is collected. A capacitor (C_{SH}) represents net positive charge stored in the sheath. Divertor plates are electrically at ground potential, (c) governing equations of Staebler and Hinton cast into a dimensionless form.

and hence possibly to ELMs, than the flat land with lower sheath potential. This inference is tested against experimental observations. The system parameters, γ and Θ, have been determined in "ELMing" and ELM-free states from measurements of T_h, T_c, j_{sat} by the Langmuir probe diagnostic [2] and the electron temperature and density in the outboard SOL above mid-plane by the Thomson scattering diagnostic [2]. A system state determined at a few ms before the onset of an ELM, which may manifest conditions more prone to ELM, is represented by a red dot in the plot. A state, determined well before the onset of an ELM (which is also shortly after the immediately preceding ELM), may manifest conditions less prone to ELM ("ELM-free" state), with forces to ELM having just been spent, and is represented by a dark blue dot. States determined at arbitrary time points in an L-mode discharge (ELM-free states) are represented by light blue dots. The two groups of dots seem to occupy more or less distinct regions according to this test, though of a limited scope, with red dots at higher normalized ion sheath potential than blue (dark and light) dots. These observations are suggestive of the involvement of sheath breakdown in the onset stage of the ELM.

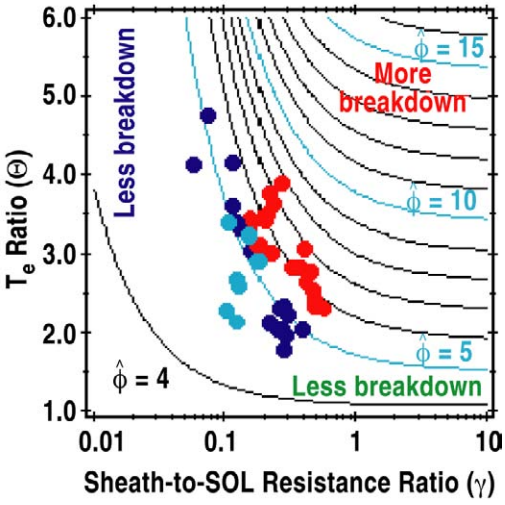

Fig. 4. Contour plot of normalized ion sheath potential, $\hat{\phi}_c$, in the system parameter space, the sheath-to-SOL resistance ratio, γ, and hot-to-cold-sheath T_e ratio, Θ. Experimental data are overlaid: ELMing (red) and ELM-free (light and dark blue).

V. Summary

Thermoelectrically driven SOLC was observed to begin to rise, often abruptly and rapidly, before the onset of thermal collapse near the pedestal top, either preceding, or co-evolving with, other signatures of the ELM process, raising the possibility that the SOLC plays a role in triggering the ELM as well as the question as to how the SOLC could rise in the face of a constraint imposed by the ion saturation current density limit at the ion sheath. Momentary sheath breakdown, caused by a potential rise across the ion sheath, is a candidate mechanism for the initial rise of the SOLC. The sheath-breakdown hypothesis was tested by comparing the ion sheath potential computed from the Harbour-Staebler-Hinton model with experimentally determined values. Apparent separation of ELMing and ELM-free states in the dimensionless parameter space of the hot-to-cold-sheath electron temperature ratio and sheath-to-SOL resistance ratio, though based on a test of a limited scope, is suggestive that sheath breakdown may be involved in the ELM onset process. Much more work is needed to examine the veracity of this hypothesis, and progress will be reported in future publications.

This work was supported by the U.S. Department of Energy under DE-AC02-76CH03073, DE-AC03-99ER54463, DE-FG03-97ER54415 and DE-AC04-94AL85000.

[1] M.E. Fenstermacher, *et al.*, Plasma Phys. Control. Fusion **45** (2003) 1597.
[2] H. Takahashi, *et al.*, Nucl. Fusion **44** (2004) 1075.
[3] H. Takahashi, *et al.*, Proc. 30th EPS Conf. on Control. Fusion and Plasma Phys., St. Petersburg, Russia, Vol. 27A (ECA, 2003) P-3.99.
[4] P.J. Harbour, *et al.*, J. Nucl. Mater. **162-164** (1989) 236.
[5] G.M. Staebler and F.L. Hinton, Nucl. Fusion **29** (1989) 1820.

External Distribution

Plasma Research Laboratory, Australian National University, Australia
Professor I.R. Jones, Flinders University, Australia
Professor João Canalle, Instituto de Fisica DEQ/IF - UERJ, Brazil
Mr. Gerson O. Ludwig, Instituto Nacional de Pesquisas, Brazil
Dr. P.H. Sakanaka, Instituto Fisica, Brazil
The Librarian, Culham Science Center, England
Mrs. S.A. Hutchinson, JET Library, England
Professor M.N. Bussac, Ecole Polytechnique, France
Librarian, Max-Planck-Institut für Plasmaphysik, Germany
Jolan Moldvai, Reports Library, Hungarian Academy of Sciences, Central Research Institute for Physics, Hungary
Dr. P. Kaw, Institute for Plasma Research, India
Ms. P.J. Pathak, Librarian, Institute for Plasma Research, India
Dr. Pandji Triadyaksa, Fakultas MIPA Universitas Diponegoro, Indonesia
Professor Sami Cuperman, Plasma Physics Group, Tel Aviv University, Israel
Ms. Clelia De Palo, Associazione EURATOM-ENEA, Italy
Dr. G. Grosso, Instituto di Fisica del Plasma, Italy
Librarian, Naka Fusion Research Establishment, JAERI, Japan
Library, Laboratory for Complex Energy Processes, Institute for Advanced Study, Kyoto University, Japan
Research Information Center, National Institute for Fusion Science, Japan
Professor Toshitaka Idehara, Director, Research Center for Development of Far-Infrared Region, Fukui University, Japan
Dr. O. Mitarai, Kyushu Tokai University, Japan
Mr. Adefila Olumide, Ilorin, Kwara State, Nigeria
Dr. Jiangang Li, Institute of Plasma Physics, Chinese Academy of Sciences, People's Republic of China
Professor Yuping Huo, School of Physical Science and Technology, People's Republic of China
Library, Academia Sinica, Institute of Plasma Physics, People's Republic of China
Librarian, Institute of Physics, Chinese Academy of Sciences, People's Republic of China
Dr. S. Mirnov, TRINITI, Troitsk, Russian Federation, Russia
Dr. V.S. Strelkov, Kurchatov Institute, Russian Federation, Russia
Kazi Firoz, UPJS, Kosice, Slovakia
Professor Peter Lukac, Katedra Fyziky Plazmy MFF UK, Mlynska dolina F-2, Komenskeho Univerzita, SK-842 15 Bratislava, Slovakia
Dr. G.S. Lee, Korea Basic Science Institute, South Korea
Dr. Rasulkhozha S. Sharafiddinov, Theoretical Physics Division, Insitute of Nuclear Physics, Uzbekistan
Institute for Plasma Research, University of Maryland, USA
Librarian, Fusion Energy Division, Oak Ridge National Laboratory, USA
Librarian, Institute of Fusion Studies, University of Texas, USA
Librarian, Magnetic Fusion Program, Lawrence Livermore National Laboratory, USA
Library, General Atomics, USA
Plasma Physics Group, Fusion Energy Research Program, University of California at San Diego, USA
Plasma Physics Library, Columbia University, USA
Alkesh Punjabi, Center for Fusion Research and Training, Hampton University, USA
Dr. W.M. Stacey, Fusion Research Center, Georgia Institute of Technology, USA
Director, Research Division, OFES, Washington, D.C. 20585-1290

The Princeton Plasma Physics Laboratory is operated
by Princeton University under contract
with the U.S. Department of Energy.

Information Services
Princeton Plasma Physics Laboratory
P.O. Box 451
Princeton, NJ 08543

Phone: 609-243-2750
Fax: 609-243-2751
e-mail: pppl_info@pppl.gov
Internet Address: http://www.pppl.gov